Fabrication and Electrochemical Characterization of TiO_2 Three-Dimensional Nanonetwork Based on Peptide Assembly

Sung-Wook Kim, Tae Hee Han, Jongsoon Kim, Hyeokjo Gwon, Hyoung-Seok Moon, Sang-Won Kang, Sang Ouk Kim, and Kisuk Kang*

Department of Materials Science and Engineering, Korea Advanced Institute of Science and Technology (KAIST), 335 Gwahangno, Yuseong-gu, Daejeon 305-701, Republic of Korea

ABSTRACT The three-dimensional network of TiO_2 hollow nanoribbons designed from a peptide assembly using atomic layer deposition is demonstrated as a promising Li secondary battery electrode in this study. The nanoribbon network ensures effective transport of electrons and Li ions due to (i) a well-connected network of nanoribbons and (ii) the hollow structure of each nanoribbon itself, into which Li ions in the electrolyte can readily diffuse. The improved specific capacity, rate capability, and cyclability of the nanonetwork show that the utilization of a nanonetwork of individual hollow ribbons can serve as a promising strategy toward the development of high-performance electrode for Li secondary batteries.

KEYWORDS: Li secondary battery · 3-d nanostructure · TiO_2 · biotemplating · ALD

Recently, intensive research efforts have focused on nanostructured materials for various applications such as energy storage[1−10] and conversion devices,[11,12] electronic[13,14] and display devices,[15,16] and bio applications.[17,18] The unique properties that originate from the nanoscale dimension of these materials frequently provide a novel pathway to overcome the limitations of conventional bulk materials. In particular, nanostructured electrode materials have garnered a considerable amount of attention as a crucial element for the next generation of Li secondary batteries. Many nanostructured materials have been investigated such as nanowires, nanotubes, core/shell nanocomposites, and 3-d mesoporous structures.[1−10] The large surface area of the nanostructured electrode provides a large interface with electrolytes and its nanoscale dimension reduces the Li ion diffusion length required for the operation of the battery, boosting the rate capability.[5,19] The nanostructured electrode can also improve the cycle stability of a Li secondary battery by readily accommodating the strain for Li insertion/extraction and thereby preventing the undesired fractures or electronic disconnects of the electrode materials. Chan *et al.* reported enhanced electrochemical performance of the electrode composed of one-dimensional nanowires, attributing the increased performance to a better strain relaxation and firm electronic contact during discharge/charge cycles.[1,2]

This study demonstrates that an electrode architecture consisting of the three-dimensional (3-d) network of hollow nanoribbons can provide high electrochemical performance for battery operation. The proposed structure is beneficial not only because the multiple large contact areas between nanoribbons in the 3-d network provide facile electronic transport paths, but also because the unique geometry of each hollow nanoribbon allows fast Li ion transport between the electrolyte and the electrode. Unlike most reported nanotube electrodes with tunnels that are too small for a moderate amount of electrolyte to penetrate into,[20−22] the hollow space of the nanoribbons reported here has a tunnel cross-section nearly 100−200 nm in width and 20−50 nm in height. This allows the electrolyte to wet the hollow space easily, which facilitates the Li transport to occur from the inside. In addition, it is easy to accommodate the volumic change during the discharge/charge cycles due to the hollow structure.

Biotemplating is becoming a valuable means of nanofabrication. A well-defined biomolecular motif may serve as a building block for a nanoscale-ordered

*Address correspondence to matlgen1@kaist.ac.kr.

Received for review January 21, 2009 and accepted April 20, 2009.

Published online April 27, 2009.
10.1021/nn900062q CCC: $40.75

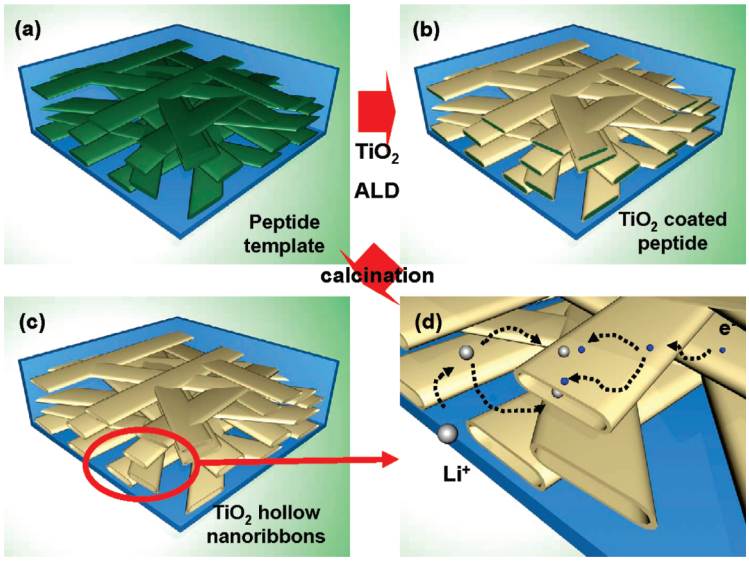

Figure 1. Schematic illustration of (a) the 3-d peptide template, (b) atomic layer deposited TiO_2 on the peptide template, (c) 3-d network structure of TiO_2 hollow nanoribbons, and (d) the Li ions and electrons transport in the TiO_2 nanonetwork electrode.

structure.[23−26] In this work, diphenylalanine is introduced as a structural motif for a highly ordered nanonetwork structure.[27] To prepare a well-defined hollow structure of a targeted electrode material as a template for a peptide structural framework, an atomic layer deposition (ALD) technique was applied. Owing to its self-limiting behavior, the thickness of the deposited material can be controlled precisely in the nanometer scale with a large area of conformality and uniformity.[28,29] Through a combination of biotemplating and ALD, a nanonetwork structured electrode was easily fabricated with the precise control of its morphology.

The functional electrode material chosen in this work is anatase TiO_2. Anatase TiO_2 is a promising anode material for Li secondary batteries owing to its high chemical stability and high capacity.[6,7,21,22,30−35] Though the working potential of anatase TiO_2 is quite high for a negative electrode material, it has the advantage of being inside the electrochemical stability window of most common electrolytes. The formation of a solid-electrolyte-interphase (SEI) layer is prohibited in the electrochemical voltage window, in which TiO_2 operates.[36] Safety accidents involving Li secondary batteries are often attributed to the thermal decomposition of the SEI layer.[37] As the safety aspects of Li secondary batteries become important, the chemical stability of TiO_2 is highly desired. The TiO_2 electrode with high safety and high capacity was prepared in a 3-d network of hollow nanoribbons, and its electrochemical properties were investigated.

RESULTS AND DISCUSSION

The fabrication strategy of the TiO_2 nanonetwork is schematically described in Figure 1. (The detailed description of fabrication methods is given in the Methods section.) The peptide template was fabricated from an organogel formed by diphenylalanine and chloroform. Evaporation of chloroform left the highly ordered 3-d nanonetwork framework (Figure 1a). The obtained peptide template was covered with 15 nm layer of TiO_2 *via* ALD at 140 °C (Figure 1b). As the obtained peptide have high thermal stability unlike other biomaterials, they can endure a further functionalization process at a relatively high ALD operating temperature (~160 °C). Then, the peptide template was removed by high temperature calcination to obtain pure TiO_2 nanonetwork structures. Given that the TiO_2 was coated onto the surface of the peptide template, the removal of the peptides by calcinations left a hollow TiO_2 structure (Figure 1c). Figure 1d schematically describes the expected transports of Li ions and electrons. Li ions can diffuse into both the outside and the inside of the hollow nanoribbons, whereas electrons can flow from one of the nanoribbons to any of the others *via* their network structure.

The microstructures of the peptide template and the corresponding TiO_2 nanonetwork are shown in Figure 2a and Figure 2b, respectively. The widths of the peptide ribbons lie within a range of 100−200 nm. The morphology of the peptide template was well replicated into TiO_2 nanonetwork morphology. The widths of the TiO_2 nanoribbons are slightly larger compared to those of the peptides, as expected. Each nanoribbon of TiO_2 is well connected to the others, forming a 3-d network structure. The inset of Figure 2b confirms that each individual nanoribbon has a hollow tubular structure. The dimension of the hollow space is comparable to that of the peptide template. The thickness of the nanoribbon was confirmed to be approximately 15 nm. The crystal structure of the TiO_2 nanonetwork was identified as an anatase phase by XRD analysis. Figure 2c shows that all diffraction peaks were well matched to the diffraction peaks of the anatase TiO_2 nanopowder. Broader peaks were observed for the hollow nanoribbons. A calculation using Scherrer's equation indicated an equivalent particle size of 12 nm,[38] which is comparable to the thickness of the wall of the hollow nanoribbons.

The electrochemical properties of the TiO_2 hollow nanoribbon network are presented in Figure 3. Generally, a reversible Li insertion/extraction reaction in anatase TiO_2 can be expressed by the following:

$$TiO_2 + xLi^+ + xe^- \leftrightarrow Li_xTiO_2 \quad (1)$$

During the Li insertion/extraction, a two-phase reaction occurs with phase equilibrium of the Li-poor $Li_{0.01}TiO_2$ phase and the Li-rich $Li_{0.55}TiO_2$ phase.[31,32] The

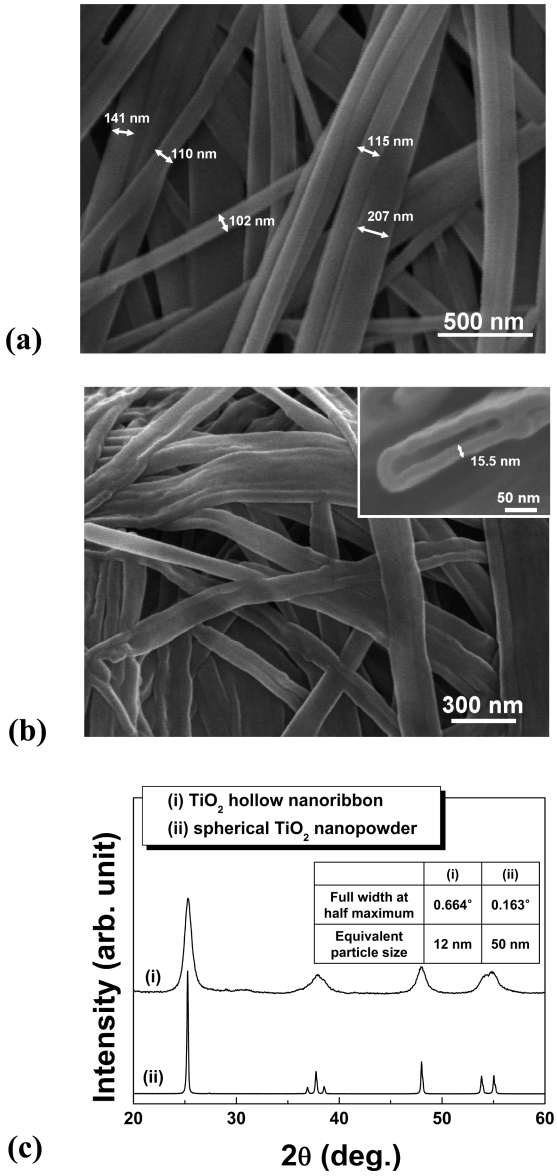

Figure 2. FESEM images of (a) the peptide template and (b) the TiO_2 nanonetwork (inset: magnified image of cross sectional TiO_2 hollow nanoribbon). (c) XRD patterns obtained from (i) the TiO_2 nanonetwork and (ii) the TiO_2 nanopowder (inset: full width at half-maximum of the (101) plane and equivalent particle size calculated from Scherrer's equation).

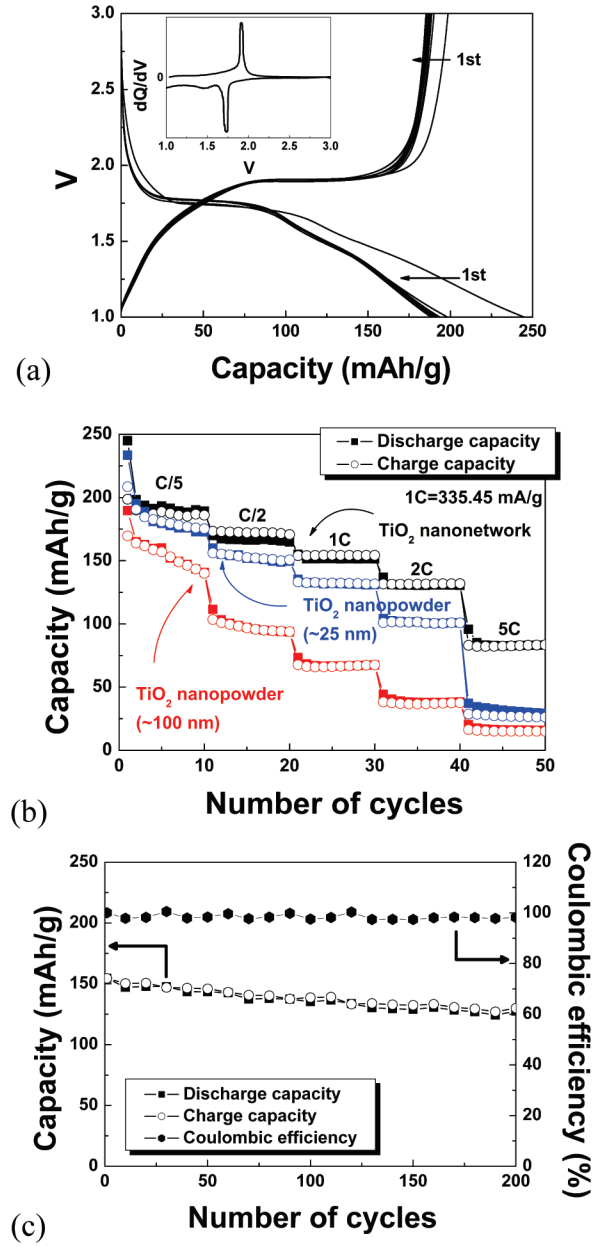

Figure 3. (a) Discharge−charge curve of the TiO_2 nanonetwork at C/5 for 10 cycles (inset: differential capacity curve of the first cycle at C/5). (b) Rate capability of the TiO_2 nanonetwork, the 25 nm- and 100 nm-TiO_2 nanopowders from C/5 to 5C for 10 cycles. (c) Specific capacity and Coulombic efficiency of the TiO_2 nanonetwork depending on the number of cycles for 200 cycles at 1C.

differential capacity curve (dQ/dV *vs* V) in the inset of Figure 3a indicates that the potential plateau is at approximately 1.72 and 1.92 V while discharging and charging, respectively. The reaction potential is in good agreement with that of reported two-phase reactions.[21,22,34] However, a significant amount of capacity was also observed below the potential of the two-phase reaction, and the total capacity is notably higher than the expected value ($x > 0.5$). The discharge capacity at the first cycle at C/5 is approximately 244.9 mAh g^{-1} ($x = 0.73$) and stabilizes at a value closed to 198.3 mAh g^{-1} ($x = 0.59$) from the second cycle. While electrolyte reduction reaction is negligible in this case due to its high operation voltage, a large irreversible capacity was observed in the first cycle. In the case of nanostructured materials, many irreversible sites for Li insertion exist such as dangling bonds and surface disordering because they have a large surface to volume ratio. Thus, it is thought that the irreversible capacity is due to the Li insertion into the irreversible sites. The short potential plateau near 1.5 V shown in Figure 3a is comparable to that of the Li insertion into the irreversible sites in the case of TiO_2 nanotubes.[21] Upon subsequent cycles, the reversibility of the Li insertion/extraction reaction is retained with $x > 0.5$. It is believed

that the surface lithiation of TiO_2 contributes to the extra capacity observed here. As the chemical potential of Li can vary significantly depending on the surrounding atomic arrangements, the under-coordinated atoms near the surface have an influence on the Li chemical potential and therefore the observed voltage and capacity. The significant surface to volume portion in the TiO_2 nanonetwork contributes to the high extra capacity in this region. Although the insertion coefficient, *x*, of the anatase TiO_2 is generally less than 0.5 due to the strong Li−Li repulsion, nanostructured anatase TiO_2 is often observed to have *x* values greater than 0.5.[21,22,33,34]

It was also noted that the major part of the total capacity was at the sloppy potential which is in contrast to the characteristic flat potential of the two-phase reaction. It is believed this cannot be attributed solely to the surface lithiation, but rather should be partly attributed to the lithiation at the phase boundary. Li atoms in the phase boundary of the two phases will experience continuous shifts of their chemical potential upon lithiation. The width of the phase boundary between the $Li_{0.55}TiO_2$ and Li_1TiO_2 phases was reported to range about 7 nm during an electrochemical reaction.[35] Considering that the wall dimension of the hollow nanoribbon is approximately 15 nm, most of the material will lie in the phase boundary. Within this phase boundary region, Li insertion/extraction does not strictly follow the two-phase behavior of a constant potential. Appreciable capacity is expected to be obtained at a potential other than the characteristic potential of the $Li_{0.01}TiO_2$−$Li_{0.55}TiO_2$ two-phase reaction for the nanoelectrodes.

The advantages of using various nanostructured electrodes for Li secondary batteries include the high rate performance due to their high specific area and short Li diffusion path.[1−10] In the case of the hollow nanoribbon network, (i) facile electronic conduction through the network and (ii) Li diffusion from both the outside and the hollow space of the tube are the important factors in the improvement of the performance besides the usual benefits from a nanosized electrode. The rate capability of the TiO_2 nanonetwork is compared with that of the TiO_2 nanopowders from C/5 to 5C for 10 cycles at each current rate in Figure 3b. The TiO_2 nanopowders were prepared with diameters of about 25 and 100 nm, which are comparable to the dimension of thickness and width of the TiO_2 nanonetwork, respectively. This figure shows that the TiO_2 nanonetwork retains superior rate capability as the current density increases by 25 times, which is in clear contrast to the TiO_2 nanopowders. The TiO_2 nanonetwork shows a higher specific capacity under all discharge/charge rates. While the specific capacities of the 25 nm- and 100 nm-TiO_2 nanopowders at 5C were as low as 34.4 and 17.6 mAh g^{-1}, respectively, the TiO_2 nanonetwork shows a 5-fold increase in the specific capacity (83.3 mAh g^{-1}) under the same rate compared to that of 100 nm-TiO_2 nanopowder. The 25 nm-TiO_2 nanopowder showed higher capacity than the 100 nm-TiO_2 nanopowder, as expected, because of its large surface area. The capacity of the 25 nm-TiO_2 nanopowder and the TiO_2 nanonetwork was comparable at C/5; however, the difference between two materials increased as the current rate increased. Also, capacity fades of both of the TiO_2nanopowders were severe compared to that of TiO_2 nanonetwork in the initial discharge/charge cycles. While the dimension of the 25-nm TiO_2 nanopowder is comparable to the thickness of the individual TiO_2 nanoribbon, it has remarkably small dimension compared to the width and length of the TiO_2 nanoribbon. In this respect, it is thought that the excellent performanceof the TiO_2 nanonetwork, especially on high current rate, originates from its unique structure, that is, 3-d network structure of hollow nanoribbons. The two-directional Li diffusion and strain relaxation improve the electrochemical performance of the TiO_2 nanonetwork.

The TiO_2 nanonetwork electrode also demonstrated excellent cyclability. Figure 3c shows the long-cycle characteristic up to 200 cycles at 1C immediately following the experiment shown in Figure 3b. The TiO_2 nanonetwork electrode retained approximately 83.2% (128.5 mAh g^{-1}) of its initial specific capacity (154.5 mAh g^{-1}) after 200 cycles. The average capacity fading per cycle was closed to 99.9% and the Coulombic efficiency was nearly 100% at each cycle. This behavior is in clearly contrast to the poor long-cycle characteristics of the 100 nm-TiO_2 nanopowder, which shows only 68.8% (50.6 mAh g^{-1}) of its initial specific capacity (73.5 mAh g^{-1}) after 200 cycles under the same condition (Supporting InformationFigure S1). Significant lattice distortion and volumic changes are induced during Li insertion/extraction between the tetragonal anatase TiO_2 and the orthorhombic $Li_{0.5}TiO_2$.[35] This can lead to fracturing of the material or a loss of electronic connectivity between the electrode particles, which can account for the capacity fade. The problem of electronic isolation is effectively prevented, we believe, due to the facile accommodation of the volumic change of the hollow nanoribbons. Unlike nanoparticles, which only expand or contract outward, the hollow structure can distribute the volumic change into both outward and inward, reducing the risk of disconnect between electrode materials. A postmortem SEM image of the TiO_2 nanonetwork shows the morphological stability even after the discharge/charge cycles shown in Figure 3 (Supporting Information Figure S2). Moreover, the high degree of the network enhances the structural stability and electronic conduction due to large area of individual nanoribbon contacts with other nanoribbons.

CONCLUSION

In summary, a hollow ribbon TiO_2 nanonetwork was fabricated successfully *via* peptide assembly and ALD. The fabricated TiO_2 nanoribbons with a highly or-

dered network structure showed superior electrochemical performance in terms of their specific capacity, rate capability, and cyclability, due to their high structural stability and high rate of ionic/electronic conduction. The utilization of a nanonetwork of hollow ribbon electrodes is suggested as a promising strategy toward the development of a high-performance electrode for Li secondary batteries.

METHODS

Diphenylalanine (Bachem) was dissolved in chloroform (Merck) to form a peptide organogel *via* sonication. The peptide nanonetwork template was simply fabricated by evaporating chloroform, which was followed by the deposition of a 15 nm layer of TiO_2 on the obtained peptide template *via* ALD under 3 Torr at 140 °C. Titanium tetra-isopropoxide (TTIP, UP Chemical) and a NH_3/O_2 mixed gas were used as a Ti precursor and a reactant gas, respectively. One ALD cycle consisted of an injection of TTIP for 5 s, an Ar purge for 20 s, an injection of the NH_3/O_2 mixed gas for 10 s, and another Ar purge for 40 s. As the deposition rate of the TiO_2 ALD was approximately 0.8 Å/cycle in this condition, 190 ALD cycles were repeated to obtain a TiO_2 thickness of 15 nm. Finally, the peptide template was removed after calcination at 400 °C for 1 h to obtain pure TiO_2 nanonetwork structures. The fabricated TiO_2 nanonetwork had powder-like form in the macroscopic scale, while it maintained 3-d nanostructure in the nanoscale as shown in Figure 2b.

The microstructures and morphologies were investigated by field-emission scanning electron microscopy (FESEM, Hitachi S-4800). The crystal structure was determined by X-ray diffraction (XRD, Rigaku D/Max 2500) with Cu Kα radiation (λ = 1.54178 Å) operating at 40 kV and 300 mA. For an electrochemical characterization, the TiO_2 nanonetwork electrode was composed of 66 wt % TiO_2 nanonetwork, 26 wt % carbon black (Super P), and 8 wt % polytetrafluoroethylene (PTFE) binder. The mass of each component was measured directly using a microbalance (Mettler Toled AB135-S/FACT). Two electrodes consisting of commercial 100 nm-TiO_2 nanopowder (Samchun Chemical) or 25 nm-TiO_2 nanopowder (Aldrich) with the same composition were also prepared for comparison. Both TiO_2 nanopowders have spherical shapes with diameters of 100−150 and 20−30 nm, respectively, which are comparable to the dimensions of the nanoribbon width and thickness, respectively (Supporting Information Figure S3). Test cells were assembled into two-electrode Swagelok-type cells with a Li metal counter electrode, a separator (Celgard 2400), and an electrolyte of 1 M $LiPF_6$ in a 1:1 mixture of ethylene carbonate and dimethyl carbonate (Techno Semichem). Discharge/charge tests were performed in the voltage range of 1−3 V at current rates from the C/5 to 5C (1C = 335.45 mA/g) using a multichannel potentio-galvanostat (WonA Tech, WBCS3000).

Acknowledgment. This work was supported by the WCU program (31-2008-000-10055-0), the General Research Grant program (R01-2008-000-10913-0), the National Research Laboratory Program (R0A-2008-000-20057-0), the 21st Century Frontier Research Programs (Center for Nanoscale Mechatronics & Manufacturing, 08K1401-01010) through the Korea Science and Engineering Foundation (KOSEF) funded by the Ministry of Education, Science and Technology (MEST). This work was supported by the Korea Research Foundation (KRF) Grant funded by the Korean Government (MEST) (KRF-2008-331-D00243).

Supporting Information Available: Specific capacity and Coulombic efficiency of the 100 nm-TiO_2 nanopowder during 200 discharge/charge cycles at 1C, SEM image of the TiO_2 nanonetwork−C composite after discharge/charge cycles shown in Figure 3, and SEM images of 100 and 25 nm TiO_2 nanopowder. This material is available free of charge *via* the Internet at http://pubs.acs.org.

REFERENCES AND NOTES

1. Chan, C. K.; Zhang, X. F.; Cui, Y. High Capacity Li Ion Battery Anodes Using Ge Nanowires. *Nano Lett.* **2008**, *8*, 307–309.
2. Chan, C. K.; Peng, H.; Liu, G.; McIlwrath, K.; Zhang, X. F.; Huggins, R. A.; Cui, Y. High-Performance Lithium Battery Anodes Using Silicon Nanowires. *Nat. Nanotechnol.* **2008**, *3*, 31–35.
3. Chan, C. K.; Peng, H.; Twesten, R. D.; Jaraush, K.; Zhang, X. F.; Cui, Y. Fast, Complete Reversible Li Insertion in Vanadium Pentoxide Nanoribbons. *Nano Lett.* **2007**, *7*, 490–495.
4. Kim, D. K.; Muralidhara, H.; Lee, H.-W.; Ruffo, R.; Yang, Y.; Chan, C. K.; Peng, H.; Huggins, R. A.; Cui, Y. Spinel LiMnO Nanorods as Lithium Ion Battery Cathodes. *Nano Lett.* **2008**, *8*, 3948–3952.
5. Poizot, P.; Laruelle, S.; Grugeon, G; Dupont, L.; Tarascon, J.-M. Nano-Sized Transition-Metal Oxides As Negative-Electrode Materials for Lithium-Ion Batteries. *Nature* **2000**, *407*, 496–499.
6. Ortiz, G. F.; Hanzu, I.; Djenizian, T.; Lavela, P.; Tirado, J. L.; Knauth, P. Alternative Li-Ion Battery Electrode Based on Self-Organized Titania Nanotubes. *Chem. Mater.* **2009**, *21*, 63–67.
7. Fu, L. J.; Zhang, T.; Cao, Q.; Zhang, H. P.; Wu, Y. P. Preparation and Characterization of Three-Dimensionally Ordered Mesoporous Titania Microparticles as Anode Material for Lithium Ion Battery. *Electrochem. Commun.* **2007**, *9*, 2140–2144.
8. Zhang, T.; Gao, J.; Zhang, H. P.; Yang, L. C.; Wu, Y. P.; Wu, H. Q. Preparation and Electrochemical Properties of Core−Shell Si/SiO Nanocomposite as Anode Material for Lithium Ion Batteries. *Electrochem. Commun.* **2007**, *9*, 886–890.
9. Fu, L. J.; Yang, L. C.; Shi, Y.; Wang, B.; Wu, Y. P. Synthesis of Carbon-Coated Nanoporous Microcomposite and Its Rate Capability for Lithium Ion Battery. *Microporous Mesoporous Mater.* **2009**, *117*, 515–518.
10. Fu, L. J.; Liu, H.; Zhang, H. P.; Li, C.; Zhang, T.; Wu, Y. P.; Holze, R.; Wu, H. Q. Synthesis and electrochemical performance of novel core/shell structured nanocomposites. *Electrochem. Commun.* **2006**, *8*, 1–4.
11. Peng, H.; Xie, C.; Schoen, D. T.; McIlwrath, K.; Zhang, X. F.; Cui, Y. Ordered Vacancy Compounds and Nanotube Formation in $CuInSe_2$-Cds Core−Shell Nanowires. *Nano Lett.* **2007**, *7*, 3734–3738.
12. Wang, C.; Waje, M.; Wang, X.; Tang, J. M.; Haddon, R. C.; Yan, Y. Proton Exchange Membrane Fuel Cells with Carbon Nanotube Based Electrodes. *Nano Lett.* **2004**, *4*, 345–348.
13. Cui, Y.; Zhong, Z.; Wang, D.; Wang, W. U.; Lieber, C. M. High Performance Silicon Nanowire Field Effect Transistors. *Nano Lett.* **2003**, *3*, 149–152.
14. Duan, X.; Huang, Y.; Lieber, C. M. Nonvolatile Memory and Programmable Logic from Molecule-Gated Nanowires. *Nano Lett.* **2002**, *2*, 487–490.
15. Talapin, D. V.; Rogach, A. L.; Korowski, A.; Haase, M.; Weller, H. Highly Luminescent Monodisperse CdSe and CdSe/ZnS Nanocrystals Synthesized in a Hexadecylamine−Trioctylphosphine Oxide−Trioctylphospine Mixture. *Nano Lett.* **2001**, *1*, 207–211.
16. Qian, F.; Gradečax, S.; Li, Y.; Wen, C.-Y.; Lieber, C. M. Core/Multishell Nanowire Heterostructures as Multicolor, High-Efficienty Light-Emitting Diodes. *Nano Lett.* **2005**, *5*, 2287–2291.
17. Patolsky, F.; Weizmann, Y.; Willner, I. Actin-Based Metallic Nanowires as Bio-Nanotransporters. *Nat. Mater.* **2004**, *3*, 692–695.

18. Lee, S. B.; Mitchell, D. T.; Trofin, L.; Nevanen, T. K.; Söderlund, H.; Martin, C. R. Antibody-Based Bio-Nanotube Membranes for Enantimeric Drug Separations. *Science* **2002**, *296*, 2198–2200.
19. Kang, K.; Ceder, G. Factors That Affect Li Mobility in Layered Lithium Transition Metal Oxides. *Phys. Rev. B.* **2006**, *74*, 094105.
20. Claye, A. S.; Fischer, J. E.; Huffman, C. B.; Rinzler, A. G.; Smalley, R. E. Solid-State Electrochemistry of the Li Single Wall Carbon Nanotubes System. *J. Electrochem. Soc.* **2000**, *147*, 2845–2852.
21. Xu, J.; Jia, C.; Cao, B.; Zhang, W. F. Electrochemical Properties of Anatase TiO_2 Nanotubes As an Anode Material for Lithium-Ion Batteries. *Electrochim. Acta* **2007**, *52*, 8044–8047.
22. Kim, J.; Cho, J. Rate Characteristics of Anatase TiO_2 Nanotubes and Nanorods for Lithium Battery Anode Materials at Room Temperature. *J. Electrochem. Soc.* **2007**, *154*, A542−A546.
23. Braun, E.; Eichen, Y.; Sivan, U.; Ben-Yoseph, G. DNA-Templated Assembly and Electrode Attachment of a Conducting Silver Wire. *Nature* **1998**, *391*, 775–778.
24. Zhang, J.; Liu, Y.; Ke, Y.; Yan, H. Periodic Square-Like Gold Nanoparticle Arrays Templated by Self-Assembled 2D DNA Nanogrids on a Surface. *Nano Lett.* **2006**, *6*, 248–251.
25. Allred, D. B.; Sarikaya, M.; Baneyx, F.; Schwartz, D. T. Electrochemical Nanofabrication Using Crystalline Protein Masks. *Nano Lett.* **2005**, *5*, 609–613.
26. Reches, M.; Gazit, E. Casing Metal Wires Within Discrete Self-Assembled Peptide Nanotubes. *Science* **2003**, *300*, 625–627.
27. Han, T. H.; Kim, J.; Park, J. S.; Park, C. B.; Ihee, H.; Kim., S. O. Liquid Crystalline Peptide Nanowires. *Adv. Mater.* **2007**, *19*, 3924–3927.
28. Chen, P.; Mitsui, T.; Farmer, D. B.; Golovchenko, J.; Gordon, R. G.; Branton, D. Atomic Layer Deposition to Fine-Tune the Surfacea Properties and Diameters of Fabricated Nanopores. *Nano Lett.* **2004**, *4*, 1333–1337.
29. Rugge, A.; Becker, J. S.; Gordon, R. G.; Tolbert, S. H. Tungsten Nitride Inverse Opals by Atomic Layer Deposition. *Nano Lett.* **2003**, *3*, 1293–1297.
30. Sudant, G.; Baudrin, E.; Larcher, D.; Tarascon, J.-M. Electrochemical Lithium Reactivity with Nanotextured Anatase-Type TiO_2. *J. Mater. Chem.* **2005**, *15*, 1263–1269.
31. Wagemaker, M.; van Well, A. A.; Kearley, G. J.; Mulder, F. M. The Life and Times of Lithium in Anatase TiO_2. *Solid State Ionics* **2004**, *175*, 191–193.
32. Koudriachova, M. V.; de Leeuw, S. W. Orthorhombic Distortion on Li Intercalation in Anatase. *Phys. Rev. B* **2004**, *69*, 054106.
33. Guo, Y.-G.; Hu, Y.-S.; Sigle, W.; Maier, J. Superior Electrode Performance of Nanostructured Mesoporous TiO_2 (Anatase). Through Efficient Hierarchical Mixed Conducting Networks. *Adv. Mater.* **2007**, *19*, 2087–2091.
34. Jiang, C.; Wei, M.; Qi, Z.; Kudo, T.; Honma, I.; Zhou, H. Particle Size Dependence of the Lithium Storage Capability and High Rate Performace of Nanocrystalline Anatase TiO_2 Electrode. *J. Power Sources* **2007**, *166*, 239–243.
35. Wagemaker, M.; Borghols, W. J. H.; Mulder, F. M. Large Impact of Particle Size on Insertion Reactions. A Case for Anatase Li_xTiO_2. *J. Am. Chem. Soc.* **2007**, *129*, 4323–4327.
36. Zhang, S.; Ding, M. S.; Xu, K.; Allen, J.; Jow, T. R. Understanding Solid Electrolyte Interface Film Formation on Graphite Electrodes. *Electrochem. Solid-State Lett.* **2001**, *4*, A206.
37. Roth, E. P.; Doughty, D. H.; Flanklin, J. DSC Investigation of Exothermic Reactions Occuring at Elevated Temperatures in Lithium-Ion Anodes Containing PVDF-Based Binders. *J. Power. Sources* **2004**, *134*, 222–234.
38. Cullity, B. D.; Stock, S. R. Elements of X-ray Diffraction, 3rd ed.; Prentice Hall: Upper Saddle River, NJ, 2001; pp 167−171..